C-ITS-enabled Antenna System for Pedestrian-to-Vehicle (P2V) Portable Communication Devices: Design and On-site tests

Narimane Awadamislmani, Divitha Seetharamdoo, Christophe Rosinski, Benoit Vuadelle

IEEE Open Journal of Intelligent Transportation Systems

Received 25 July, 2024; revised XX Month, 2024; accepted XX Month, 2024; Date of publication XX Month, 2024; date of current version XX Month, 2024.

Digital Object Identifier 10.1109/OJITS.2024.070709

C-ITS-enabled Antenna System for Pedestrian-to-Vehicle (P2V) Portable Communication Devices: Design and On-site tests

NARIMANE AWADAMISLMANI*, DIVITHA SEETHARAMDOO*, *IEEE member*, CHRISTOPHE ROSINSKI*, and BENOIT VUADELLE†

[1]COSYS-LEOST, Univ Gustave Eiffel, Villeneuve d'Ascq, F 59650, France.
[2]Autoroutes Paris Rhin Rhone (APRR), 22d Av. Lionel Terray, 69330 Jonage, France

CORRESPONDING AUTHOR: Divitha SEETHARAMDOO (e-mail: divitha.seetharamdoo@univ-eiffel.fr).

ABSTRACT Vehicular communication systems can be used to improve the safety level of road users by exchanging safety/warning messages. In this paper, we propose an antenna for a pedestrian-to-vehicle (P2V) device that provides a safety service to road workers on the highway or the road environment. A metasurface antenna system was fabricated and tested first in a controlled laboratory environment in an anechoic chamber. The device is designed to be worn close to the body of the road worker and in this framework the specific absorption rate (SAR) has to be evaluated and compared to the threshold values recommended by standards. Field tests results in an environment representative of the highway are conducted at the Transpolis test tracks are also provided to validate the performances of our system. It is shown that the proposed antenna system consisting of two monopoles backed by a metasurface reflector is an excellent candidate for P2V communications based on IEEE 802.11p systems with desirable radiation pattern, polarization, and safety limits.

INDEX TERMS Cooperative Intelligent Transport Systems (C-ITS), Pedestrian to Vehicle (P2V), Vulnerable Road Users (VRU), ITS-G5, 802.11p, circularly polarized monopole antenna, metasurface reflector, specific absorption rate (SAR).

I. INTRODUCTION

COOPERATIVE intelligent transport systems (C-ITS) are being deployed in Europe [1], [2], for both road infrastructures [3] and vehicles. This deployment facilitates the development of next-generation cooperative systems, improving safety [4], efficiency, and harmonious co-existence among different transport methods.

Several recent and ongoing projects are addressing associated with the challenges with the deployment of C-ITS. For example, C-Roads France [5], is a C-ITS pilot deployment project that focuses on the development and experimentation of innovative road solutions. One of the key usecases explored in this project is the pedestrian-to-vehicle (P2V) communication systems to protect vulnerable road users (VRU). The integration of VRUs into C-ITS [6] presents a promising approach to improve the safety of road workers on highways and in scenarios where the number of accidents is high [7].

Various communication technologies have been employed to design VRU protective equipment and can be classified in two categories, namely (i) common and non-dedicated communication technologies, such as Bluetooth [8], Wi Fi [9]–[11], Cellular (MNO) networks (LTE-3G, 4G) [12]–[14], and GNSS (e.g., GPS) [15], and (ii) dedicated communication technologies specifically designed for transportation safety applications. They are based on standards like IEEE 802.11p or ITS-G5 [16]–[20], as well as the newer cellular-based communication (C-V2X, NR-V2X, 5G-V2X) technology [21].

P2V communications and VRU safety is a rather recent research topic. The solutions proposed to establish P2V communication consist in using a personal ITS Station such

as tags [], smartphones [], and dedicated devices []. It should be noted that, to date, no existing portable dedicated VRU communicating devices have been proposed.

Our research work focuses on the use of the already-deployed IEEE 802.11p communication standard for the design of VRU protective equipment specifically designed to be worn by road workers in highway environments. This system should enable road workers to broadcast alerts to neighboring vehicles and infrastructure in case of potentially dangerous situations, thus ensuring timely and effective reaction within a minimum distance of 300 meters. This novel approach has been implemented as part of the C-Roads France project and supported by APRR on its pilot site.

The VRU device consists of an ITS-G5 communication system with an integrated antenna system facilitating message broadcasting. The successful implementation of the P2V communication based on the 802.11p standard relies on the use of compatible and high-performing antennas. [22].

Antenna specifications accounting for a high variability in position and orientation of the roadworkers with respect to vehicles and roadside units makes the selection of an appropriate antenna type challenging. Directive antennas [23]–[25] could be a good candidate for their high gain and extended communication range, were also employed for SAR reduction. However, their drawback is the suppression of lateral radiation [26], which can significantly impact the performance of the system in certain use-case scenarios.

In this paper, an antenna system composed of two metasurface-reflector antennas [27]–[31] placed back to back is proposed to preserve lateral radiation while addressing the requirements in terms of Specific Absorption Rate (SAR) levels. To handle the integration of the omnidirectional antenna system close to the human body, the SAR should be minimized to ensure compliance with the recommended threshold values given by relevant safety standards and recommendations [32] and [33].

The paper is organised as follows. In section II, we define the use case of the C-Roads project with a portable VRU device based on C-ITS systems for roadworkers on the highway. In section III, antenna specifications and integration scenarios to account for the VRU implementation requirements are described. Section IV presents a detailed description of the antenna system, design methodology and structure. In Section V, numerical and experimental results in anechoic chamber are presented. Section VI, focuses on on-site system evaluation in terms of received power level, describing the measurement scenarios, experimental setup, and the results obtained. Finally, section VII compares and analyses the performance of our antenna system with other research works in other applicative fields.

II. P2V Communication system based on IEEE 802.11p: use case description

A highway environment including a roadworker equipped with a VRU communication device based on IEEE 802.11p communication protocols is illustrated in Figure 1. The VRU

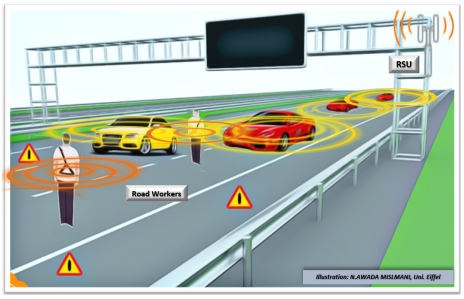

FIGURE 1. Illustration of the communication system 802.11p-based P2V in highway, where the road workers, vehicles and infrastructures are equipped with 802.11p communication protocol

device should allow for the broadcasting of messages in the highway or road environment, where the road workers, vehicles and infrastructures are all equipped with 802.11p communication systems. This device consists of a ITS-G5 communication system with an integrated antenna system.

For road worker safety, it is essential that this antenna system simultaneously accounts for two challenges, namely, achieving a minimum broadcast range of 300 meters to ensure effectiveness under adverse highway conditions, accounting for reaction times at speeds of 130 km/h; and enabling predominantly line-of-sight signal propagation. These characteristics are inline with the underlying principles of Intelligent Transportation Systems (ITS), particularly the ITS-G5 communication standard where low latency, direct and real-time communication between VRU, vehicles and infrastructure are required.

III. Antenna specifications and integration

The functional requirements derived from ITS-G5 can be subdivided on two categories as depicted in Figure 2. The first one is related to the communication protocol and the second one depends on the applicative scenario where the communication system is to be deployed.

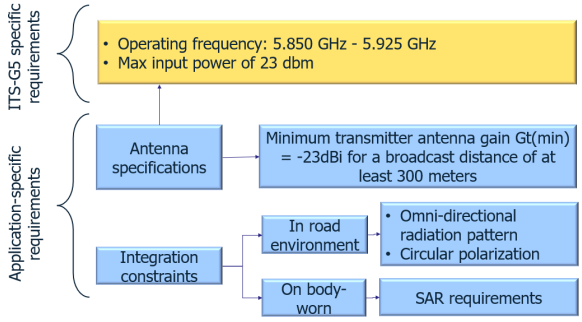

FIGURE 2. Functional requirements derived from communication system ITS-G5. (i) application-specific requirements and (ii) Communication specific ITS-G5.

The environment-related integration constrainsts and typical antenna specifications are detailed in the following subsections.

A. Integration constraints

For the considered scenario, the placement and integration of the antenna on the body of roadworkers are critical considerations to ensure effective communication while ensuring safety. Throughout the design and evaluation of the P2V device, a specific integration scenario is considered. It is shown in Figure 3.

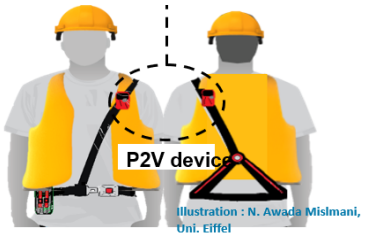

FIGURE 3. Body worn P2V device (antenna integration scenario, where the antenna is placed on the human body in a back-to-back configuration).

It consists of two body-worn antennas. One antenna element is placed on the top left of the back of the body, while the other antenna element is placed on the front of the body. Both are then interfaced with the communication system through a power splitter. In the integration scenario we proposed, the miniaturization of the antenna was not a critical requirement. However, the antenna gain was identified as crucial to minimize power consumption and ensure the autonomy of the device.

To handle the integration of the VRU antenna system close to the human body, the Specific Absorption Rate (SAR) should be minimized to ensure compliance with the recommended threshold values given by relevant safety standards and recommendations of the International Commission on Non-Ionizing Radiation Protection (ICNIRP) and the Federal Communications Commission (FCC) [32], [33] set at 0.4 W/kg for occupational exposure [32] and [33].

B. Antenna specifications

The successful implementation of the P2V communication system based on 802.11p standard, relies on the use of compatible and high-performing antennas. To meet the specific requirements derived from the ITS-G5 communication system, the following specifications of the antenna system are derived:

- Operating frequency band: the antenna should operate within the specified frequency band of ITS-G5 communication (e.g., 5.850 GHz - 5.925 GHz), enabling efficient signal transmission and reception.
- Radiation pattern: due to the demanding nature of the road-worker environment, it is essential for the antennas to have specific spatial radiation selectivity. An omnidirectional antenna can prove to be a good candidate such that signal reception degradation in other directions can be avoided.
- Polarization: the axial ratio (AR) of the antenna should be less than 3 dB to achieve circular polarization, which facilitates predominantly line-of-sight propagation. Additionally, this feature is important since the proximity of lossy and high dielectric materials, such as water and the human body, is known to create depolarization of waves
- Gain: the minimum transmitter antenna gain is determined through an analytical approximation at a frequency of 5.9 GHz. It is given by $G_{t(\min)}$ = -23 dBi considering a separation distance of 300 m between the transmitting and receiving antennas. The calculation is performed using the Friis equation. Even though the minimum required gain is low, a good level of acceptable gain is necessary since it would result in less power consumption and thus a higher autonomy level of the portable device.

IV. Antenna system design

A. Design methodology

The design of the antenna system proposed follow the steps depicted in figure 4.

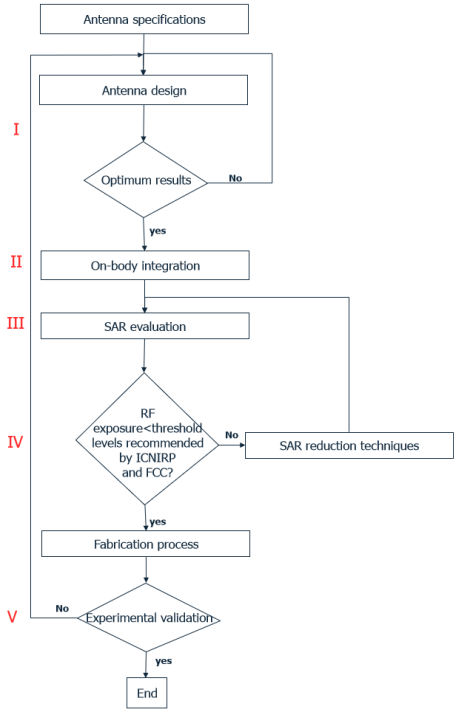

FIGURE 4. Design Methodology Steps: (1) Geometric optimization for 5.9 GHz resonance and circular polarization; (2) Investigation of human body effect; (3) Numerical evaluation of Specific Absorption Rate (SAR) compliance; (4) Introduction of metasurface-based reflector for human body radiation control; (5) Experimental validation in controlled lab and real-world field tests at Transpolis.

In the initial stage of the design process, optimization of the geometrical dimensions was carried out to achieve resonance at 5.9 GHz while ensuring circular polarization. Subsequently, the impact of human body interaction on the

system was thoroughly investigated. A metasurface reflector is thus introduced to control the radiation in the human body. To comprehensively assess the performance of the proposed metasurface reflector, a numerical evaluation of Specific Absorption Rate (SAR), which quantifies human body exposure, is conducted in accordance with relevant safety standards. Furthermore, experimental validation of the VRU prototype is performed in both a controlled laboratory environment in anechoic chamber, and in real-world field tests conducted at the Transpolis.

B. Antenna system structure

The antenna system considered in this research work is illustrated in Figure 5.

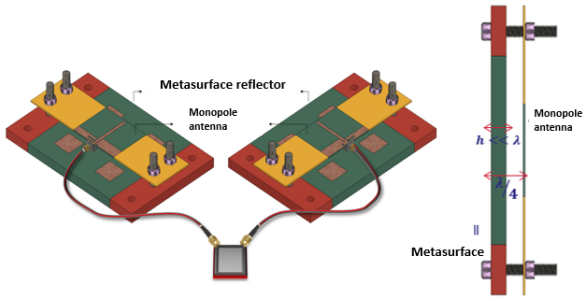

FIGURE 5. Overview of the antenna system structure, consisting of two microstrip-monopole antennas backed by metasurface reflectors with a gap of $\lambda/4$.

It consists of a two microstrip-monopole antenna system backed by metasurface reflectors. The gap between the antenna and the metasurface, was chosen to the point where the distance between the human body and the antenna is almost equal to $\lambda/4$. These antennas are connected to the electronic device through conductive wires. Designed to be worn on the back to back of road workers' bodies, as depicted in the integration scenario shown in the preceding section (Section III).

1) CP monopole antenna

A circularly-polarized monopole antenna integrated is designed and simulated using CST suite 2021, as shown in Figure. 6, with dimensions listed in the table 1.

The CP monopole antenna is composed of stub metallic radiating elements, an asymmetric ground plane [27], [28], and a substrate (FR4, dielectric material of permittivity of 4.4, and a thickness of 1.6 mm). By embedding a slit on the ground plane, this antenna achieves a broad impedance bandwidth and circular polarization (CP) [30], [31]. The CP monopole antenna is fed by a coplanar waveguide (CPW) terminated by a discrete 50 ohm feeding port and a dielectric material (permittivity of 4.4) as the substrate.

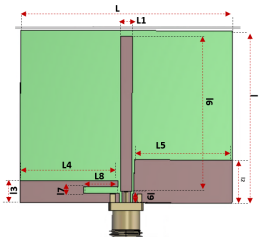

FIGURE 6. Illustration of the CP monopole antenna in free space. It consists of stub metallic radiating elements, an asymmetric ground plane with an embedded slit, and an FR4 dielectric substrate (permittivity: 4.4, thickness: 1.6 mm). Fed by a coplanar waveguide (CPW).

TABLE 1. Antenna parameters.

Parameters	Values (mm)
Antenna width (L)	40.7
Antenna length (W)	33
Stub width (l1)	2.2
Stub length (l6)	29.7
Left ground length (l3)	4.18
Left ground width (l4)	18.81
Right ground width (l5)	18.81
Right ground length (l2)	6.49
Slit length (l7)	1.32
Slit width (l8)	6.6
Feed length (l9)	1.76
Height (h)	1.6

2) Metasurface reflector

A metasurface of reflection coefficient with 0° phase based on patch antenna was integrated, which has the the capability of reflecting energy with zero phase shifts. So that the backward energy toward human body will be redirected to opposite direction resulting in increasing the radiation in the human body [34]–[36]. The unit cell of the reactive impedance metasurface (RIM) and its corresponding equivalent circuit are depicted in Figure 7.

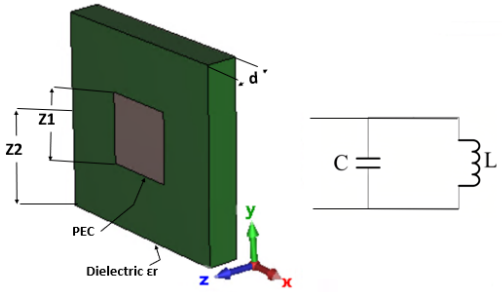

FIGURE 7. The geometry of the metasurface as a Floquet cell with periodic boundaries conditions, where Z_1 is the length of the patch, Z_2 is the distance between the unit-cells and d is the thickness of the substrate. On the left side, its equivalent LC circuit

There are many parameters that contribute to the final expression of the phase of the reflection coefficient ϕ of a reactive impedance metasurface. It is given by:

$$\phi = 2arctan(\frac{1}{Z_0}\frac{X_c X_L}{X_c - X_L}), \tag{1}$$

where Z_0 is the wave impedance of free space, X_L is the inductive reactance defined as:

$$X_L = \frac{Z_0}{\sqrt{\epsilon_r}} tan(\frac{2\pi f\sqrt{\epsilon_r}}{c} d), \tag{2}$$

and X_C is the capacitive reactance:

$$X_c = \frac{1}{2\pi f C}. \tag{3}$$

an upper estimation of the capacitance C can be calculated by considering the two metal patches as a coplanar stripline; the capacitance per meter can therefore be given by:

$$C_0 = \frac{\epsilon K(\sqrt{1 - Z_r}}{Z_r} \tag{4}$$

where K is the complete elliptic integral of first kind and ϵ is the effective dielectric constant, which should account for the fact that the electric field is distributed partly in the dielectric and partly in free space:

$$\epsilon = \epsilon_0 \frac{\epsilon_r + 1}{2} \tag{5}$$

and Z_r is the geometrical parameter given by:

$$Z_r = \frac{Z_1}{Z_2} \tag{6}$$

where Z_1 is the length of the patch and Z_2 is the distance between the metamaterials

The previous equations show that the phase of the reflection coefficient for a reactive impedance metasurface is affected by various parameters. To provide a comprehensive understanding of the design process, three matrices were introduced and visually presented in Figure 8.

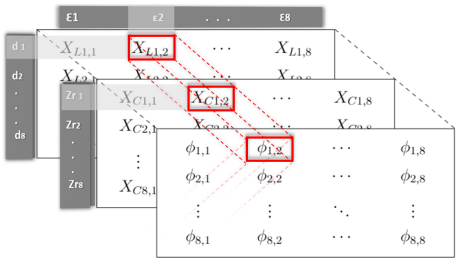

FIGURE 8. 3 matrices show the phase of the reflection coefficient which is a function of the inductance X_L and the capacitance X_C, Which in turn depend on three physical parameters such as, thickness of the substrate, the permittivity and the size of the metallic patch

Through the use of these matrices, one can effectively select the appropriate physical characteristics of the unit cell to engineer a reactive impedance metasurface (RIM) with a desired reflection phase.

In this study, a phase of 0° was chosen as the reference for determining the metasurface parameters. To achieve this, X_L was carefully selected, and an estimated value of d was derived considering the parameter ϵ_r, which represents the relative permittivity of the substrate. The capacitive reactance X_C was then chosen to provide a range of values for $Z_r = \frac{Z_1}{Z_2}$, taking into account the parameter ϵ_r.

To validate the analytical results, the design was simulated using CST microwave studio at a frequency of 5.9 GHz. The simulation yielded an optimized configuration with $Z_r = \frac{Z_1}{Z_2} = 0.443$, where $Z_1 = 13.6$, $Z_2 = \frac{\lambda}{50}$, and $d = 6.1$ mm. These parameters were specifically adjusted for a lossless substrate of permittivity $\varepsilon_r = 4.4$. Figure 9 shows the phase calculated in degrees with respect to frequency. The phase

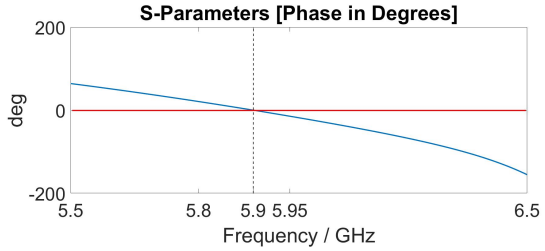

FIGURE 9. Simulated reflection phase at 5.9 GHz. This figure illustrates the simulated reflection phase characteristics of the metasurface at $\phi = 0$. The analysis is conducted using a Floquet cell model with periodic boundary conditions.

of the reflection coefficient of the unit cell presents $\phi = 0$ at the operating frequency of 5.9 GHz in agreement with the analytical approach.

V. Description of the human body model

Since the antenna was designed to operate with a P2V communication system, its performance must be evaluated when it is close to the human body due to partial absorption and reflection of electromagnetic energy.
To speed up the computation, the human body was simplified into a three-layer tissue numerical model for simulation, with dimensions of 200 mm x 200 mm that represents the real human environment, as shown in Figure 10.

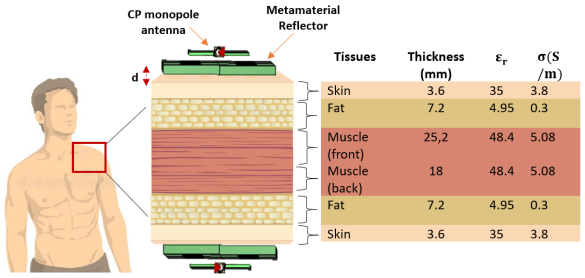

FIGURE 10. Simulated human body tissue environment. A simplified three-layer tissue numerical model (200 mm x 200 mm) representing the real human environment for simulation purposes.

It is made up of skin, fat, and muscle. The electrical lengths of each of these layers are listed in the table in Figure 10 and are defined by the electrical properties and thickness of the corresponding tissues layers that are obtained from a realistic phantom model (the Zubal phantom) [37], at 5.9 GHz.

VI. Numerical and experimental validation in anechoic chamber

A. Description of the P2V prototype

To validate the performance of the P2V antenna system, a prototype is fabricated and tested. The antenna prototype is shown in Figure 11.

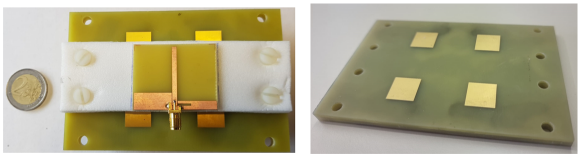

FIGURE 11. Fabricated antenna system backed by metasurface reflectors on FR4 substrate, with dimensions of 11.5 x 7.5 cm. (a) Antenna system (b) Metasurface.

The prototype consists of the three layers : (i) the monopole antenna printed on FR4 substrate, (ii) Rohacell foam (permittivity $\varepsilon = 1.1$) of thickness 5 mm, (iii) the metasurface, baked by metallic ground plane. The antenna consists in 35 µm-thick copper printed on an FR4 substrate of permittivity ($\varepsilon = 4.4$, $\tan\delta = 0.018$) and thickness of 1.6 mm. The metasurface shown in Figure 11(b) is printed on an FR4 substrate of thickness 6.1 mm. The transmission line is then terminated with a 50Ω 3.5 mm SMA connector to feed the antenna.

B. Description of measurement set-up

1) S_{11} and Radiation pattern

The design prototype is measured with a Vector Network Analyzer (VNA) to validate the impedance matching.

The radiation pattern measurement was performed in an anechoic chamber at 5.9 GHz in both E-plane and H-plane. Figure 12 shows the measurement setup for the radiation pattern in the far field of the anechoic chamber.

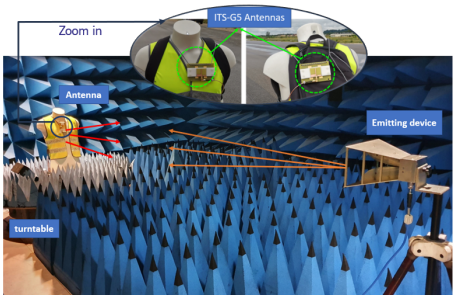

FIGURE 12. Antenna pattern measurement setup in anechoic chamber.

An linear-polarised emitting antenna is placed at a distance of 3 meters from our proposed antenna, which is integrated on the front side of a human-body simulating mannequin used in our experimentation. The mannequin is filled with a tissue simulating liquid (TSL) for frequency of 5800 MHz with a tolerance 10%. The dielectric parameters of the body simulation fluid are defined in the FCC KDB publication 865664 and correspond to a permittivity ϵ_r=48.2 and a conductivity σ=6 S/m. These liquids are representative of the human body and are based on the permittivity and conductivity of the muscles. The mannequin is positioned on a turntable, such that the radiated fields can be measured with respect to angular positions.

2) Axial ratio

To assess the circular polarisation (CP) property of the antenna, the axial ratio must be measured. The measurement setup in the anechoic chamber is shown in Figure 13. The

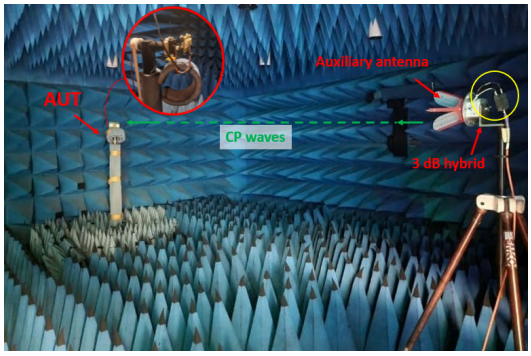

FIGURE 13. Axial ratio measurements setup in anechoic chamber. Measurements are conducted using the polarization rotation method [38]. An open boundary quad-ridged horn antenna serves as the auxiliary antenna, connected to a 3dB hybrid to generate CP waves. The antenna under test (AUT) is installed on an Axis Antenna Positioner and positioned on a turntable.

measurements are carried out using the polarisation rotation method, as described in [38]. An open boundary quad-ridged horn antenna operating from 2 GHz to 18 GHz frequency range was used as the auxiliary antenna. A 3dB hybrid is connected to the auxiliary antenna to generate CP wave. The Antenna Under Test (AUT) is installed on an Axis Antenna Positioner and positioned on a turntable.

C. Results

Figure 14 shows the simulated and measured reflection coefficient bandwidth. The S_{11} is shown to be less than -10 dB in the operating frequency band ranging from 5.8 GHz to 5.95 GHz. The normalized radiation patterns obtained from numerical simulation were then validated by the experimentations performed in the anechoic chamber at 5.9 GHz in both the E-plane (for $\phi = 90°$) and H-plane ($\phi = 0°$). The cross and co-polarization are also measured. These results are shown in Figure 15.

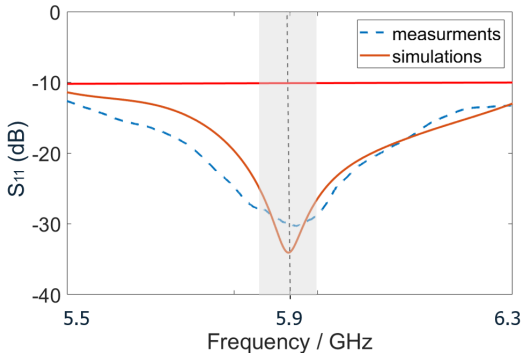

FIGURE 14. Simulated Return Loss, validated by experimental. The gray part represents the frequency band of 5.85-5.95 GHz

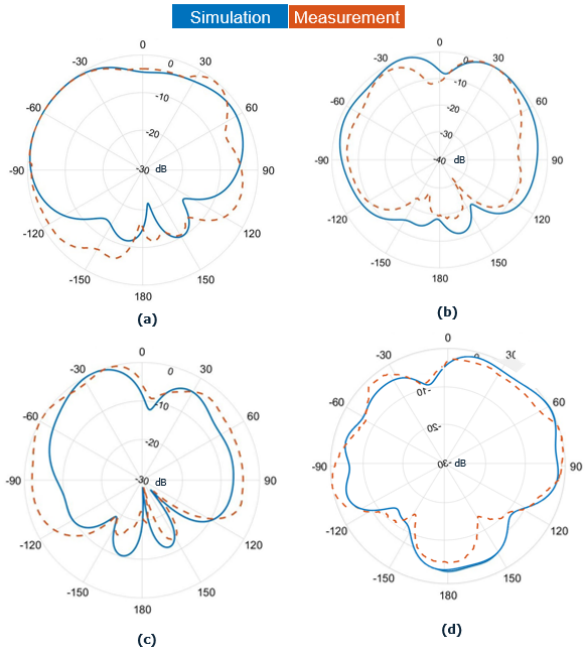

FIGURE 15. Simulation validates with experimental measurements in E-plane Cross polarization (a) and Co polarization (b) at 5.9 GHz, in H-plane Cross polarization (c) and Co polarization (d) at 5.9 GHz.

The measured results are in good agreement with simulations in both the E- and H-planes. While the measured radiation pattern matches the simulated radiation pattern in the direction of the main lobe, some discrepancies occurred in the radiation pattern measurement in the back lobe. This difference is mostly due to the slight differences in the human body model used for simulations and the mannequin available for experimentations. Simulating exactly the same scenario would require too high computational complexity. The measured back lobe results are considered acceptable for our application.

The measured axial ratio of the circularly-polarized monopole antenna and its corresponding simulation results are depicted in Figure 16. The results obtained from the polarization rotation method agree with the simulation results. The 3-dB axial ratio bandwidth, both simulated and measured, is 11.6 % within the ITS-G5 band.

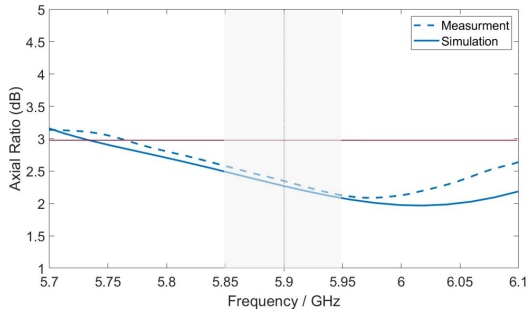

FIGURE 16. Simulated axial ratio, validated by experimental.

D. Numerical SAR assessment

The SAR value was obtained by simulations performed according to the averaging method stated in IEEE/IEC 62704-1 [39], for an input power of 23 dBm and a frequency of 5.9 GHz. The limit for the average SAR is 10 W/Kg for the parts of the human body treated as extremities, such as hands, wrists, feet, ankles, and pinnae. For an antenna positionned close to the body tissues, the SAR distribution calculated and averaged over 10g of inside body tissue at 5.9 GHz is depicted in Figure17.

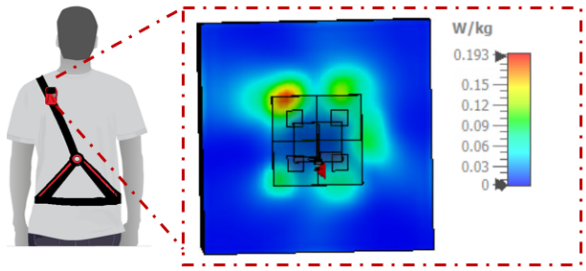

FIGURE 17. SAR distribution on body tissue at 5.9 GHz with antenna and metasurface. The simulation indicates a maximum SAR value of 0.193 W/kg, which complies with safety standards (ICNIRP and FCC) set at 0.4 W/kg for occupational exposure.

The maximum SAR value of 0.193 W/kg obtained from simulation, shows that it is well within the limits of the safety standards of ICNIRP and FCC [32], [33] set at 0.4 W/kg for occupational exposure. The results thus confirm that the metasurface antenna system prototyped is a good candidate to be deployed on road workers in the highway environment for C-ITS-enabled P2V devices.

VII. On-site evaluation

A. Measurement scenario

An on-site evaluation of the P2V device integrating our antenna was performed in controlled highway environment of Transpolis Fromentaux in collaboration with the partners Transpolis [40] and Autoroute Paris Rhin Rhone (APRR). The runway used at Transpolis is the Highway runway

offering 5 Traffic lanes over a length of 900m. A speed of 130 km/h can be reached at the entrance of the straight line.

B. Experimental Set-up

Figure 18 depicts the measurement setup used for on-site testing. The transmitting system is integrated on our

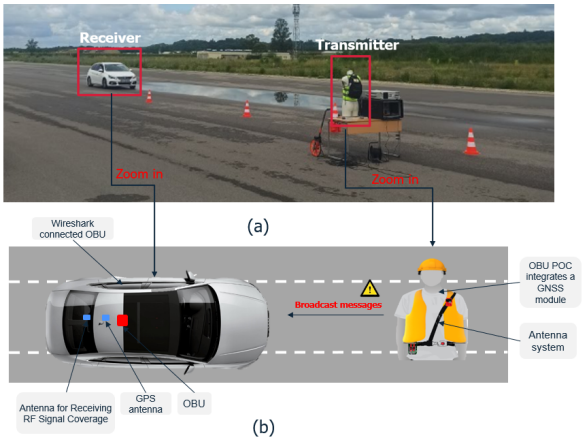

FIGURE 18. On-site test setup in TRANSPOLIS FROMENTAUX highway environment. The setup consists of: (i) Transmitting antenna system and (ii) AREA van equipped with an 802.11p onboard unit (OBU) for receiving.

mannequin; it consists in our antenna prototype under test connected to an ITS-G5 Communication module (designed by Lacroix city V2X) and a GPS antenna. This system broadcasts messages, such as CAM (Cooperative Awareness Message) and a specific DENM (Decentralized Environmental Notification Message) announcing the presence of a roadworker on the highway. The later will be received based on the geo-localization of the vehicle with respect to the roadworker. On the receiving end, the measurement test involves an APRR car equipped with an 802.11p Onboard Unit (OBU), a PC sniffer running Wireshark, a GPS antenna and an omni-directional ITS-G5 antenna mounted on the roof of the car. This system operates as a receiver to accurately assess the radio coverage within a 1 km area. Both CAM and DENM messages broadcoasted from the P2V Antenna system are received. Additionally, the system is capable of recording the received power level, facilitating the evaluation of signal strength and the power thresholds during the measurement process.

C. Measurement results

During the measurement tests, three orientations of our antenna prototype are considered, as shown in Figure 19.

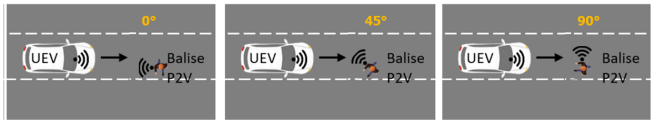

FIGURE 19. Considered orientations of our antenna prototype under test: $0\,\mathrm{deg}$**,** $45\,\mathrm{deg}$**, and** $90\,\mathrm{deg}$**.**

The received signal strength indicator (RSSI) measured by an 802.11p system onboard a fast-moving vehicle over a range of 70 km/h to 130 km/h, has been measured over a distance of 1 km. The results are summarized in Table 2.

TABLE 2. Received signal strength level vs. distance (dBV/km) from moving vehicles

Angle	Speed (km/h)	Outbound (m)
0°	70	822
0°	130	795
45°	70	848
45°	130	838
90°	70	733
90°	130	778

The maximum RSSI reached varies between 730 and 848 m. The P2V antenna system thus demonstrated a maximum broadcast distance of 860 meters, higher than the specified distance of 300 meters by a factor of 2.75.

VIII. Discussion

In this section, we analyze and discuss the performances of our proposed antenna system designed for VRU wearable devices used by dynamic road workers on highways. Our antenna system is compared to two configurations: integration with a conventional metallic reflector instead of a metasurface and a system of two back-to-back conventional patch antennas. Antenna system performances in terms of frequency band, circular polarization, and lateral direction coverage are considered. Finally, a discussion considering recent state-of-the-art antennas reported in the literature is presented to highlight the novelty of our proposal.

It can be demonstrated that there is less deformation of the radiation pattern and the matching is better with a metasurface reflector rather than a conventional metallic reflector. Simulation results for two antenna system configurations: (i) our proposed system, which consists of a monopole antenna integrated with a metasurface reflector, and (ii) a configuration with a conventional metallic reflector with a gap of $\lambda/4$ are illustrated in Figure 20.

Figure 20(a), indicate that the antenna system backed by a metasurface presents higher reflection coefficient bandwidth in ITS-G5 band with S_11 less than -10 dB and an axial ratio less that 3dB. Additionally, our antenna system achieves a higher lateral direction coverage (from 60° to 120° and -120° to -60°) with differences as high as 9.48 dBi as shown in figure 20(b).

A. Comparison of a our proposed antenna to a system of two back-to-back conventional patch antennas

Optimising the radiation pattern in the lateral directions can prove to be tedious; the monopole antenna is a good candidate despite the relative complexity to standard antennas such as a patch antenna which naturally integrates a ground plane as back reflector. For the sake of comparison, a set of

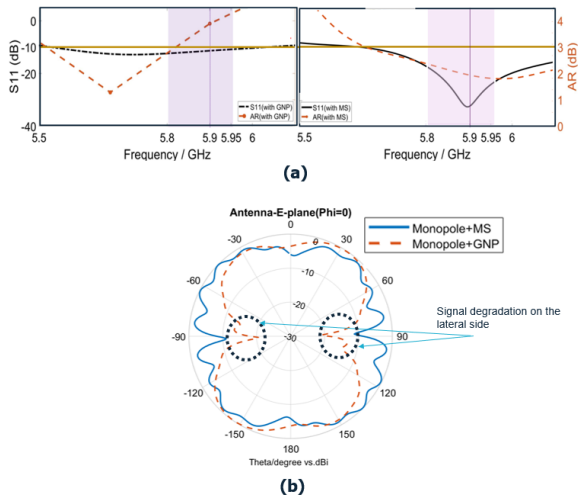

FIGURE 20. **(a) Comparison of simulated antenna characteristics (return loss and axial ratio) between the antenna backed by a metallic reflector and the antenna backed by our proposed metasurface. (b) Simulated radiation pattern in the E-plane at 5.9 GHz for both antenna system configurations with the human body effect.**

simulated radiation patterns both in 2D and 3D are illustrated in Figure 21.

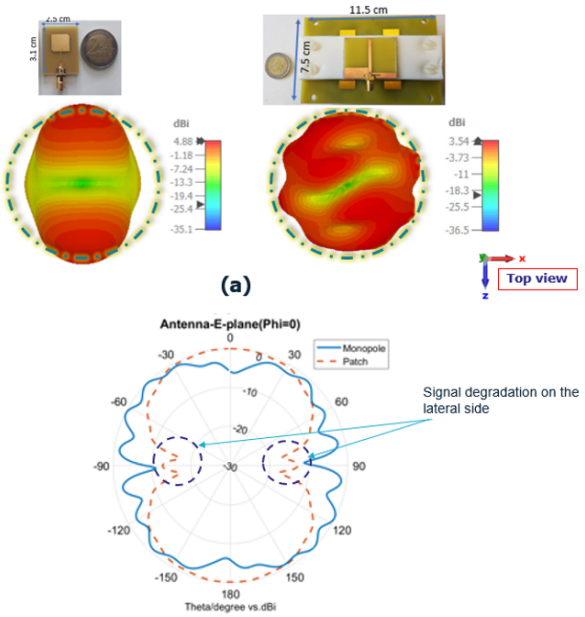

FIGURE 21. **(a) Simulated normalized 3D radiation patterns: Left shows the pattern for the patch antenna system (comprising two patch antennas placed back to back with the human body), and right shows the radiation pattern for our proposed antenna system (utilizing the same configuration). (b) Simulated normalized 2D radiation pattern in the E-plane at 5.9 GHz with a highlight on the lateral radiation level differences.**

The top-view of the 3D radiation patterns (Figure 21(a)) demonstrate that our antenna system presents a circular shaped pattern while the patch antenna system presents an elliptical shaped pattern with minimal radiation on the sides. A normalized 2D radiation pattern in the E-plane (depicted in Figure 21(b)) corresponding to the 3D top view allows for better appreciation of the lateral directions coverage range (from 60° to 120° and -120° to -60°). The patch antenna system achieves a lower coverage in the lateral direction compared to our proposed antenna system with a maximum difference of 6.6 dBi.

B. Comparison with existing antennas from the literature

The performances of our proposed antenna system with recent state-of-the-art wearable antenna reported in the literature are compared. Table 3 provides a detailed comparison in terms of radiation, circular polarisation characteristics.

TABLE 3. **Performance Comparison of our Antenna Systems with literature.**

Ref.	Freq. (GHz)	AR BW (%)	S_{11} BW (%)	Gain (dBi) / Rad. Eff. (%)	Lateral directions	SAR (W/Kg) over (10g)
[41]	5.16	18.3	18.3	6.2/90	no	chest: 0.097
[42]	4	12.5	12.5	5.2/80	no	0.066
[43]	5.7	11.44	18.18	7.6/94.6	no	chest 0.137
[44]	5.8	9.1	CP	7.2/60.2	no	0.043 (1g)
[45]	5.8	15.9	2.72	5.2/79	no	0.18
[46]	5.8	3.97	2.93	2.1/72.6	yes	0.118 (1g)
Proposed	5.9	20.13	11.6	3.54/82.6	yes	0.193

These antennas partially fulfil the requirements of the VRU device antenna. Indeed, antennas referenced in [41]–[44] exhibit favorable characteristics such as small size, low axial ratio, and low SAR but they suffer from signal degradation in the lateral direction, which makes them unsuitable for integration into our VRU device. Because of the dynamic movement and varying positions of the VRU with respect to the roadside and cars, good lateral direction radiation characteristics are required. In comparison to the omni-directional button antenna referenced in [45], our proposed antenna demonstrates higher gain, efficiency, and wider bandwidth in terms of axial ratio (AR) and S_{11}. This should result in improved received signal strength, transmission reliability, and overall communication system performance, making our antenna design the best candidate for the dynamic and challenging environments encountered by VRU devices.

IX. Conclusion

In this paper, we propose a novel antenna system for body worn pedestrian-to-vehicular (P2V) devices to support experimentation and deployment of C-ITS solutions to improve safety and efficiency in road transportations. The antenna system consists of two circularly-polarized monopoles backed by metasurface reflector. The effect of the human body was included throughout the design process.

The antenna system shows a very good matching in the operating frequency band of the ITS-G5 from 5.8 GHz to 5.95 GHz with reflection coefficient less than -10dB as well as a circular polarization at 5.9 GHz with an axial ratio of 2.1 dB. A metasurface antenna system prototype was fabricated and tested in the anechoic chamber. The experimental results obtained are in good agreement with the simulated ones. In addition, the proposed antenna system shows an omni-directional radiation pattern in both H and E planes. The SAR distribution averaged over 10g of inside body tissue at 5.9 GHz, was obtained by simulation according to the FCC standard and with the averaging method stated in IEEE/IEC 62704-1, for an input power of 23 dBm. The maximum SAR value of 0.193 W/kg was obtained from simulation showing that it is well within the limits of the safety standards recommended by ICNIRP. A thorough comparison between our antenna system and other systems shows that two monopole antennas backed by a metasurface is the best candidate for this application.

Moreover, onsite test campaigns in an environment representative of a highway where C-ITS roadside units, vehicular onboard units and the VRU devices are deployed have shown that our proposed antenna system achieved a maximum broadcast distance of 860m which is 2.75 times the minimum specified distance of 300 m. The proposed antenna system is thus fully compatible with the specifications derived from communication system 802.11p in terms of omni-directional radiation pattern, circular polarization, gain, matching and safety RF exposure limits.

Acknowledgment

This work has been performed in the framework of the European projects C-Roads-France and Indid project partially funded by the Connecting EU facility of the European Union and coordinated by the French Ministry of Ecological Transition. Support from the RITMEA and IMITECH projects co-financed by the European Union with the European Regional Development Fund, the French state and the Hauts de France Regional Council is acknowledged. The authors would like to thank Vincent Recipon from LaCroix City V2X and E. Chateauroux (Transpolis SAS) for their active contributions in the Pedestrian to vehicle usecase specification, communication system design and on-site testing.

REFERENCES

[1] A. Kotsi, E. Mitsakis, and D. Tzanis, "Overview of c-its deployment projects in europe and usa," in *2020 IEEE 23rd International Conference on Intelligent Transportation Systems (ITSC)*, 2020, pp. 1–6.

[2] K. Sjoberg, P. Andres, T. Buburuzan, and A. Brakemeier, "Cooperative intelligent transport systems in europe: Current deployment status and outlook," *IEEE Vehicular Technology Magazine*, vol. 12, no. 2, pp. 89–97, 2017.

[3] V. Maglogiannis, D. Naudts, S. Hadiwardoyo, D. van den Akker, J. Marquez-Barja, and I. Moerman, "Experimental v2x evaluation for c-v2x and its-g5 technologies in a real-life highway environment," *IEEE Transactions on Network and Service Management*, vol. 19, no. 2, pp. 1521–1538, 2022.

[4] A. Matin and H. Dia, "Impacts of connected and automated vehicles on road safety and efficiency: A systematic literature review," *IEEE Transactions on Intelligent Transportation Systems*, vol. 24, no. 3, pp. 2705–2736, 2023.

[5] C-roads project website. [Online]. Available: https://www.c-roads.eu/pilots/coremembers/france/Partner/project/show/c-roads-france.html

[6] J. Scholliers, M. van Sambeek, and K. Moerman, "Integration of vulnerable road users in cooperative its systems," *European Transport Research Review*, vol. 9, p. 15, 2017.

[7] Edgar snyder associates website, resources: Road construction accident statistics. [Online]. Available: https://www.edgarsnyder.com/resources/road-construction-accident-statistics

[8] J. J. Anaya, E. Talavera, D. Giménez, N. Gómez, F. Jiménez, and J. E. Naranjo, "Vulnerable road users detection using v2x communications," in *2015 IEEE 18th international conference on intelligent transportation systems*. IEEE, 2015, pp. 107–112.

[9] J. J. Anaya, P. Merdrignac, O. Shagdar, F. Nashashibi, and J. E. Naranjo, "Vehicle to pedestrian communications for protection of vulnerable road users," in *2014 IEEE Intelligent Vehicles Symposium Proceedings*. IEEE, 2014, pp. 1037–1042.

[10] K.-S. Huang, P.-J. Chiu, H.-M. Tsai, C.-C. Kuo, H.-Y. Lee, and Y.-C. F. Wang, "Redeye: Preventing collisions caused by red-light running scooters with smartphones," *IEEE Transactions on Intelligent Transportation Systems*, vol. 17, no. 5, pp. 1243–1257, 2016.

[11] S. Fujikami, T. Sumi, R. Yagiu, and Y. Nagai, "Fast device discovery for vehicle-to-pedestrian communication using wireless lan," in *2015 12th Annual IEEE Consumer Communications and Networking Conference (CCNC)*. IEEE, 2015, pp. 35–40.

[12] C. Sugimoto, Y. Nakamura, and T. Hashimoto, "Prototype of pedestrian-to-vehicle communication system for the prevention of pedestrian accidents using both 3g wireless and wlan communication," in *2008 3rd International Symposium on Wireless Pervasive Computing*. IEEE, 2008, pp. 764–767.

[13] Z. Liu, L. Pu, Z. Meng, X. Yang, K. Zhu, and L. Zhang, "Pofs: A novel pedestrian-oriented forewarning system for vulnerable pedestrian safety," in *2015 International Conference on Connected Vehicles and Expo (ICCVE)*, 2015, pp. 100–105.

[14] U. Hernandez-Jayo, I. De-la Iglesia, and J. Perez, "V-alert: Description and validation of a vulnerable road user alert system in the framework of a smart city," *Sensors*, vol. 15, no. 8, pp. 18 480–18 505, 2015. [Online]. Available: https://www.mdpi.com/1424-8220/15/8/18480

[15] B. Schaffer, G. Kalverkamp, M. Chaabane, and E. M. Biebl, "A cooperative transponder system for improved traffic safety, localizing road users in the 5 ghz band," *Advances in Radio Science*, vol. 10, pp. 39–44, 2012. [Online]. Available: https://ars.copernicus.org/articles/10/39/2012/

[16] X. Wu, R. Miucic, S. Yang, S. Al-Stouhi, J. Misener, S. Bai, and W.-h. Chan, "Cars talk to phones: A dsrc based vehicle-pedestrian safety system," in *2014 IEEE 80th Vehicular Technology Conference (VTC2014-Fall)*. IEEE, 2014, pp. 1–7.

[17] D. Thielen, T. Lorenz, M. Hannibal, F. Köster, and J. Plättner, "A feasibility study on a cooperative safety application for cyclists crossing intersections," in *2012 15th International IEEE Conference on Intelligent Transportation Systems*. IEEE, 2012, pp. 1197–1204.

[18] J. J. Anaya, E. Talavera, D. Gimenez, N. Gomez, F. Jimenez, and J. E. Naranjo, "Vulnerable road users detection using v2x communications," in *2015 IEEE 18th International Conference on Intelligent Transportation Systems*, 2015, pp. 107–112.

[19] M. Kwakkernaat, F. Ophelders, J. Vissers, D. Willemsen, and P. Sukumar, "Cooperative automated emergency braking for improved safety beyond sensor line-of-sight and field-of-view," in *Proceedings of the FISITA 2014 World Automotive Congress, Maastricht, The Netherlands*, 2014, pp. 2–6.

[20] A. Tahmasbi-Sarvestani, H. Nourkhiz Mahjoub, Y. P. Fallah, E. Moradi-Pari, and O. Abuchaar, "Implementation and evaluation of a cooperative vehicle-to-pedestrian safety application," *IEEE Intelligent Transportation Systems Magazine*, vol. 9, no. 4, pp. 62–75, 2017.

[21] S. Zeadally, M. A. Javed, and E. B. Hamida, "Vehicular communications for its: Standardization and challenges," *IEEE Communications Standards Magazine*, vol. 4, no. 1, pp. 11–17, 2020.

[22] M. Jutila, J. Scholliers, M. Valta, and K. KujanpÃ¤Ã¤, "Its-g5 performance improvement and evaluation for vulnerable road user safety services," *IET Intelligent Transport Systems*, vol. 11, no. 3, pp. 126–133, 2017. [Online]. Available: https://ietresearch.onlinelibrary.wiley.com/doi/abs/10.1049/iet-its.2016.0025

[23] D. Duraj, M. Rzymowski, K. Nyka, and L. Kulas, "Espar antenna for v2x applications in 802.11 p frequency band," in *2019 13th European Conference on Antennas and Propagation (EuCAP)*. IEEE, 2019, pp. 1–4.

[24] K. Maliatsos, L. Marantis, P. S. Bithas, and A. G. Kanatas, "Hybrid multi-antenna techniques for v2x communications—prototyping and experimentation," in *Telecom*, vol. 1, no. 2. Multidisciplinary Digital Publishing Institute, 2020, pp. 80–95.

[25] M. F. Foysal, S. Mahmud, and A. Baki, "A novel high gain array antenna design for autonomous vehicles of 6g wireless systems," in *2021 International Conference on Green Energy, Computing and Sustainable Technology (GECOST)*. IEEE, 2021, pp. 1–5.

[26] P. Dhanesh, M. J. George, and B. Anoop, "A review on sar reduction methods used for mobile application," *IOSR Journal of Electronics and Communication Engineering (IOSR-JECE)*, vol. 10, no. 5, pp. 25–27, 2015.

[27] Q. Chen, H. Zhang, and L.-c. Yang, "Compact cpw-fed dual-band linearly and circularly polarized monopole antenna for wimax/wlan applications," in *2018 International Conference on Microwave and Millimeter Wave Technology (ICMMT)*. IEEE, 2018, pp. 1–3.

[28] C.-J. Wang and K.-L. Hsiao, "Cpw-fed monopole antenna for multiple system integration," *IEEE Transactions on Antennas and Propagation*, vol. 62, no. 2, pp. 1007–1011, 2013.

[29] A. Ghobadi and M. Dehmollaian, "A printed circularly polarized y-shaped monopole antenna," *IEEE Antennas and Wireless Propagation Letters*, vol. 11, pp. 22–25, 2011.

[30] G. Li, H. Zhai, T. Li, L. Li, and C. Liang, "A compact antenna with broad bandwidth and quad-sense circular polarization," *IEEE Antennas and Wireless Propagation Letters*, vol. 11, pp. 791–794, 2012.

[31] H. Ren, Y. Yu, and Z. Shen, "Broadband circularly-polarised antenna consisting of four notch slot radiators," *Electronics letters*, vol. 48, no. 23, pp. 1447–1449, 2012.

[32] I. C. on Non-Ionizing Radiation Protection *et al.*, "Guidelines for limiting exposure to electromagnetic fields (100 khz to 300 ghz)," *Health physics*, vol. 118, no. 5, pp. 483–524, 2020.

[33] R. E. Fields, "Evaluating compliance with fcc guidelines for human exposure to radiofrequency electromagnetic fields," *OET bulletin*, vol. 65, no. 10, 1997.

[34] K. Zhang, P. J. Soh, and S. Yan, "Meta-wearable antennas—a review of metamaterial based antennas in wireless body area networks," *Materials*, vol. 14, no. 1, p. 149, 2021.

[35] H. Yalduz, B. Koç, L. Kuzu, and M. Turkmen, "An ultra-wide band low-sar flexible metasurface-enabled antenna for wban applications," *Applied Physics A*, vol. 125, no. 9, pp. 1–11, 2019.

[36] U. Ali, S. Ullah, J. Khan, M. Shafi, B. Kamal, A. Basir, J. A. Flint, and R. D. Seager, "Design and sar analysis of wearable antenna on various parts of human body, using conventional and artificial ground planes," *Journal of Electrical Engineering and Technology*, vol. 12, no. 1, pp. 317–328, 2017.

[37] G. Z. et al, "The zubal phantom," in *Yale University School of Medicine, New Haven, CT USA*.

[38] B. Li, "Axial ratio measurements of circularly polarised antennas based on polarisation rotation," *IET Microwaves, Antennas & Propagation*, vol. 12, no. 15, pp. 2379–2382, 2018.

[39] I. C. on Non-Ionizing Radiation Protection *et al.*, "Determining the peak spatial-average specific absorption rate (sar) in the human body from wireless communications devices, 30 mhz to 6 ghz - part 1: General requirements for using the finite-difference time-domain (fdtd) method for sar calculations," *Health physics*, vol. ., no. ., pp. 1–86, 27 Oct. 2017.

[40] Transpolis. [Online]. Available: https://transpolis.fr/fr/

[41] U. Ullah, I. B. Mabrouk, and S. Koziel, "A compact circularly polarized antenna with directional pattern for wearable off-body communications," *IEEE Antennas and Wireless Propagation Letters*, vol. 18, no. 12, pp. 2523–2527, 2019.

[42] Z. H. Jiang and D. H. Werner, "A compact, wideband circularly polarized co-designed filtering antenna and its application for wearable devices with low sar," *IEEE Transactions on Antennas and Propagation*, vol. 63, no. 9, pp. 3808–3818, 2015.

[43] Y. B. Chaouche, M. Nedil, I. B. Mabrouk, and O. M. Ramahi, "A wearable circularly polarized antenna backed by amc reflector for wban communications," *IEEE Access*, vol. 10, pp. 12 838–12 852, 2022.

[44] H. Yang, X. Liu, Y. Fan, and L. Xiong, "Dual-band textile antenna with dual circular polarizations using polarization rotation amc for off-body communications," *IEEE Transactions on Antennas and Propagation*, vol. 70, no. 6, pp. 4189–4199, 2022.

[45] Z. H. Jiang, Z. Cui, T. Yue, Y. Zhu, and D. H. Werner, "Compact, highly efficient, and fully flexible circularly polarized antenna enabled by silver nanowires for wireless body-area networks," *IEEE Transactions on Biomedical Circuits and Systems*, vol. 11, no. 4, pp. 920–932, 2017.

[46] X. Hu, S. Yan, J. Zhang, V. Volski, and G. A. E. Vandenbosch, "Omnidirectional circularly polarized button antenna for 5 ghz wban applications," *IEEE Transactions on Antennas and Propagation*, vol. 69, no. 8, pp. 5054–5059, 2021.